

1 **Simulating the 1976 Teton Dam Failure using GeoClaw**
2 **and HEC-RAS and comparing with Historical**
3 **Observations**

4 **H. R. Spero¹, D. Calhoun², and M. Schubert³**

5 ¹Boise State University, Department of Geosciences
6 ²Boise State University, Department of Mathematics
7 ³HDR Engineering Inc., Boise, Idaho

8 **ORCID Identifiers**

- 9 • H. R. Spero: 0000-0002-0912-9340
10 • D. Calhoun: 0000-0002-6005-4575
11 • M. Schubert: 0000-0001-5509-7637

12 **Key Points:**

- 13 • GeoClaw results within acceptable range for dam failure downstream modeling
14 with comparison to historical data and HEC-RAS results.
15 • Novel use of Lagrangian gauges to track downstream eddying in GeoClaw soft-
16 ware.
17 • Fundamental Teton Dam failure benchmark problem used for comparison of soft-
18 ware and prepared for future dam failure modeling applications.

19 **Keywords**

20 GeoClaw; flood numerical modeling; Teton Dam; HEC-RAS; dam failure

Corresponding author: Hannah Spero; Current Affiliation: University of Notre Dame, Email:
hspero@nd.edu

21 **Abstract**

22 Dam failures occur worldwide, often from factors including aging structures, ex-
 23 treme hydrologic loading, and design oversights related to the changing climate. Under-
 24 standing and mitigating risk to downstream inhabited areas require developing and im-
 25 proving low-cost high-fidelity tools, such as numerical models, which allow emergency
 26 managers to predict the consequences of dam failures better. Two-dimensional (2D) depth-
 27 averaged hydraulic models can provide valuable insights into the importance of breach
 28 parameters or downstream flow characteristics, but historical studies considering historic
 29 failures using real topographies are less common in literature. This study compares Geo-
 30 Claw, a 2D hydraulic model with novel adaptive mesh refinement capabilities, to an industry-
 31 standard software HEC-RAS (Hydrologic Engineering Center - River Analysis System)
 32 using the 1976 Teton Dam failure as a case study. The suitability of GeoClaw for dam
 33 failure modeling is determined based on its capability to resolve inundation extent and
 34 flood wave arrival times. This study performs sensitivity analyses of the HEC-RAS model
 35 to compare an instantaneous dam breach assumption with a time-dependent breach for-
 36 mation for quantifying the model uncertainty. We find the 2D GeoClaw dam-break model
 37 results compare reasonably with historical gauge records and field observational data and
 38 HEC-RAS results. The model demonstrates stability and relatively low computational
 39 costs. Our findings highlight opportunities for future work, with the GeoClaw software
 40 performance supporting continued studies to evaluate performance. Outcomes of this study
 41 will assist dam owners, floodplain managers, and emergency managers by providing an
 42 additional tool for estimating the impacts of dam failures to protect lives and infrastruc-
 43 ture downstream.

44 **1 Introduction**

45 Dam failures have caused some of the most significant disasters associated with the
 46 failure of human-made systems, and the aging dam population is expected to increase
 47 by 65% in failures in the next decade (ASDSO, 2021). Although dam failures are rel-
 48 atively rare, with one large-scale dam failure per year, climate change studies suggest
 49 catastrophic dam failures are likely to become more common due to increased hydrologic
 50 loading, as most of the aging dam population was not designed to consider global warm-
 51 ing; earthen dams being especially vulnerable (Stanford University, 2018; Loza & Fidélis,
 52 2021; Boulange et al., 2021). The United States (US) has 91,000 dams that impound 965,606 km
 53 of rivers, with an average of ten reported dam failures occurring every year (ASDSO, 2021).
 54 Despite advancements in technology and current monitoring tools in place, catastrophic
 55 dam failures continue to occur. Two recent examples are the Edenville and Sanford Dam
 56 failures in Michigan, United States (ASCE, 2021).

57 Computational models are crucial tools for assessing the downstream consequences
 58 of potential catastrophic dam failures. While a fully three-dimensional (3D) simulation
 59 of a flooding event would be prohibitive for all but the fastest supercomputers, two-dimensional
 60 (2D), depth-averaged numerical models have been shown to provide robust results that
 61 agree well with observations and can be run efficiently on standard laptops or desktop
 62 workstations (Néelz et al., 2010). Because the downstream flow conditions are often phys-
 63 ically complex however, it is critical to investigate the importance and sensitivity of key
 64 parameters such as roughness coefficient and dam failure mode in these 2D hydraulic mod-
 65 els. Software validation and documentation of model sensitivity provides the end user
 66 confidence in model results (Néelz et al., 2010; Psomiadis et al., 2021).

67 Many studies have generally assumed that an instantaneous dam breach can be used
 68 instead of a more realistic time-dependent dam breach (Wurbs, 1987; Valiani et al., 2002).
 69 However, ongoing research is investigating the validity of this assumption due to limited
 70 scientific evidence to substantiate that assumption with earthen dam breaches (Yi, 2011;
 71 Bhandari, 2017). We test the validity of the instantaneous breach assumption by com-

72 paring the downstream consequences between a time-dependent and an instantaneous
 73 dam failure mode for the Teton Dam failure.

74 This study compares the research code GeoClaw developed initially at the University
 75 of Washington (Berger et al., 2011; George, 2011; Turzewski et al., 2019), to HEC-
 76 RAS (Hydraulic Engineering Center - River Analysis System), developed by the Army
 77 Corps of Engineers (Brunner, 2002; Urzică et al., 2021). A key advantage of the Geo-
 78 Claw software is that it can adaptively refine the numerical mesh used to track flood pro-
 79 gression over large topographic domains. HEC-RAS conversely has a sophisticated Graph-
 80 ical User Interface (GUI) and advanced tools for implementing different modes of dam
 81 failure and roughness coefficients, for example. GeoClaw has been validated for use in
 82 tsunami modeling, it has not been widely used for dam failure modeling, so this study
 83 tests the appropriateness of using GeoClaw for academic dam failure studies, in compari-
 84 son to the HEC-RAS software, which serves as an industry standard for dam failure mod-
 85 eling.

86 Actual dam failure events can offer a robust source of observational data for use
 87 in validating high-performance computational codes. Examples of commonly used dam
 88 failures events used as software benchmark problems include the Malpasset dam failure,
 89 Baldwin Hills reservoir failure, and Vajont dam failure case studies (Aureli et al., 2021;
 90 Begnudelli & Sanders, 2007; Bosa & Petti, 2011; Urzică et al., 2021; Hervouet & Petit-
 91 jean, 1999; Biscarini et al., 2016; Valiani et al., 2002; Gallegos et al., 2009). In this study,
 92 we use the 1976 Teton Dam failure (US), an event that predominantly formed the ba-
 93 sis for the understanding of dam failures (Reclamation, 1976, 2006; ASDSO, 2021). The
 94 Teton Dam domain provides complex topography to challenge 2D solvers and has a wealth
 95 of data associated with the event because of its historical importance. The Teton Dam
 96 failure is a demanding and unique case study for computational code comparison that
 97 requires simulating flood wave propagation over complex terrain.

98 This study answers two guiding questions through an examination of the hydraulics
 99 and a thorough comparison of two 2D modeled downstream flow regimes of the Teton
 100 Dam failure:

- 101 • How does GeoClaw compare with HEC-RAS using the Teton Dam benchmark prob-
 102 lem? To answer this question this study uses a comparison criteria including flood
 103 wave arrival times, lateral inundation extent, and flow depths.
- 104 • How sensitive is the Teton Dam HEC-RAS model and what is the model uncer-
 105 tainty? To answer this question four sensitivity analyses were performed evalu-
 106 ating the models sensitivity to (i) computational mesh cell size (ii) Manning's rough-
 107 ness coefficient (iii) the time-dependent or instantaneous dam breach assumption
 108 (iv) reservoir volume size.

109 **2 Background**

110 **2.1 Teton Dam Site and Historic Failure**

111 The Teton Dam geometry and flood were well-documented by the Bureau of Recla-
 112 mation (Reclamation), the United States Geological Survey (USGS), and local residents,
 113 allowing for a robust account describing the event (Reclamation, 2006, 1976; Carter, 1976;
 114 USGS, 1976).

115 Furthermore, this event has been studied using one-dimensional models and has
 116 helped form the basis for the understanding of earthen dam failures (Blanton, 1977; Sny-
 117 der, 1977; Brown, 1977; Fread, 1977; Thomas, 1977; Macchione & Sirangelo, 1990; Gund-
 118 lach & Thomas, 1977; Balloffet & Scheffler, 1982). The Teton Dam is not yet considered
 119 a common physical model for dam failure modeling, and has not yet been numerically
 120 modeled in 2D. Therefore, this study provides contributions to the field and new anal-

121 yses for determining the numerical algorithms' effectiveness for dam-break modeling (Aureli
 122 et al., 2021). Further, the data from this paper provides full documentation of the con-
 123 solidated Teton Dam failure data for future work in preparing the Teton Dam failure as
 124 a more common a benchmark problem for code comparison (Spero, Hannah and Calhoun,
 125 Donna and Schubert, Michael, 2021).

126 The Teton Dam Site consists of the Teton River Canyon (21 km upstream from Rexburg,
 127 Idaho) and the Teton Dam in Eastern Idaho, US. The Teton River canyon is narrow at
 128 the upstream end, 30.5 km from its mainstem near Victor, ID. The canyon becomes grad-
 129 ually wider downstream with a decreasing slope (Magleby, 1981; Reclamation, 2000; Pierce
 130 et al., 1992; Williams et al., 1982). Reclamation commissioned the embankment dam to
 131 provide irrigation and flood control along with wildlife mitigation measures (Reclamation,
 132 1976). At time of failure, the Teton Dam was one of the tallest dams in the US in 1976,
 133 with a crest height of 93 m at elevation 1626 m above mean sea level (MSL). The length
 134 of the crest of the dam was 914.4 m, and the width of the crest was 10.7 m. Although
 135 the dam was designed to store a volume of $3.55 \times 10^8 \text{ m}^3$ (288,000 acre-ft, it only reached
 136 $2.89 \times 10^8 \text{ m}^3$ (234,260 acre-ft) before failure (Reclamation, 2006). At the time of fail-
 137 ure, the Teton Reservoir had 82 m Water Surface Elevation (WSE) above the river bed
 138 (2006).

139 At 7:30 on 5 June 1976, a piping failure occurred in the earthen dam when the un-
 140 derlying porous basaltic rock allowed water to seep through the embankment carrying
 141 away the core material under extreme pressures, resulting in a catastrophic breaching
 142 of the dam (Reclamation, 1976). The resulting flood extended 250 km downstream un-
 143 til the American Falls Reservoir captured the flow (6 June 1976). The flooding destroyed
 144 downstream infrastructure and caused 11 deaths (Nagel & Ptak, 2021; Reclamation, 1976).
 145 From Reclamation analyses, the significant internal destruction of the dam occurred over
 146 the period of one hour between 11:00 - 11:57 on 5 June 1976 (Solava & Delatte, 2003;
 147 Reclamation, 1976).

148 2.2 A Computational Model of Dam Failure

149 2.2.1 Shallow Water Equations Application in Dam Break Modeling

150 It is widely accepted that the Shallow Water wave Equations (SWE) are viable as
 151 the mathematical formulation for resolving dam failure flood regimes, beginning with
 152 critical work in the 1970s (Martin & Zovne, 1971; Strelkoff et al., 1977; Keefer & Simons,
 153 1977; Shigeeda et al., 2001; Kocaman et al., 2021). General agreement exists that the
 154 SWE can be used to describe dam-break waves over natural topography as they com-
 155 bine computational efficiency and accurate reconstruction of real-world flow regimes (Balloffet
 156 & Scheffler, 1982; Hervouet & Petitjean, 1999). Although the SWE do not contain hy-
 157 drostatic terms and therefore cannot explicitly represent the flow behavior directly at
 158 the dam-break site due to extreme vertical accelerations. Downstream the SWE assump-
 159 tions, such as the pressure distribution being hydrostatic and turbulence neglection are
 160 recovered and can accurately estimate flow regimes (Garcia-Martinez et al., 2009). Ad-
 161 ditionally, although specific 3D models can simulate dam-breaks (including depicting pres-
 162 sures using hydrostatic terms), the computational cost of a 3D model for simulating dam-
 163 break phenomena is substantial. For example, 3D models often require higher resolution
 164 topography, they solve additional terms at each time step, and require technological ad-
 165 vances in high-performance computing or access to computing resources one might not
 166 have for parallel processing (Hu et al., 2018; Capasso et al., 2021).

The mathematical description of the SWEs are expressed in conservation form as

$$\begin{aligned} h_t + \nabla \cdot \mathbf{u}h &= 0 \\ (hu)_t + \nabla \cdot \left(h\mathbf{u} \otimes \mathbf{u} + \frac{1}{2}gh^2\mathcal{I} \right) &= gh\nabla b + \mathbf{S} \end{aligned} \quad (1)$$

where $h(x, y, t)$ is the height of the water column, $\mathbf{u} = (u(x, y, t), v(x, y, t))$ are depth averaged horizontal velocities, and $b(x, y)$ is the topography. Additional source terms $\mathbf{S}^f \equiv (S_x^f, S_y^f)$ model friction with the floodplain and are typically expressed as

$$\begin{aligned} S_x^f &= n^2 u \sqrt{u^2 + v^2} h^{-\frac{4}{3}} \\ S_y^f &= n^2 v \sqrt{u^2 + v^2} h^{-\frac{4}{3}} \end{aligned} \quad (2)$$

where n is the Manning's n roughness coefficient.

For dam failure modeling, several computational models implement the SWEs for simulating downstream flooding dynamics allowing for hazard assessment, mitigation planning, and academic studies of flow regime (Yakti et al., 2018; Shrestha et al., 2020; George & Nair, 2015; Kumar et al., 2017). Below, we describe the GeoClaw, and HEC-RAS models with additional details are summarized in Table 1.

2.2.2 HEC-RAS

First released in 1995 by the US Army Corp of Engineers (USACE) (Brunner, 2002), HEC-RAS v.5.0.7 (2019) has the capability of performing 2D computations based on depth-averaged flow (Brunner, 2016; USACE, 2019). HEC-RAS uses an implicit finite volume method and can take larger time steps than would normally be required by an explicit method (CivilGEO, 2021). Recent work includes simulation of a levee breach and resulting inundation, where a combined 1D/2D HEC-RAS approach was used and illustrated good agreement with observed data, and complex 2D models (Dasallas et al., 2019). A similar hydrodynamic approach was used, based on the HEC-RAS v.5.0.7 model to reproduce the Ukai Dam (India) flood event (Patel et al., 2017). This simulation highlighted the broad capabilities of HEC-RAS 5.0.7 for flood modeling and inundation mapping studies from dam failure (2017). Additionally, HEC-RAS has been used as a standard benchmark tool to test the performances of other models as it is both open-source and easily accessible through a Graphical User Interface (GUI) (Costabile et al., 2020; Brunner, 2016).

2.2.3 GeoClaw

The GeoClaw software v.5.8 (2020) is part of the open-source software package Clawpack (Conservation Laws Package). GeoClaw has been used in previous studies for storm surge, outburst floods, debris flow, (Mandli & Dawson, 2014; George, 2011; Turzewski et al., 2019; MacInnes et al., 2013; Arcos & LeVeque, 2015), and has been extensively tested and validated for tsunami simulations (González et al., 2011). Based on a high-resolution finite volume algorithm described in (LeVeque, 2002), GeoClaw is unique in that it can dynamically adapt mesh resolution to follow solution features of interest. In the dam failure modeling, GeoClaw can be tuned to use high-resolution grids only in flooding regions where the water column height is larger than zero. Using this refinement strategy, GeoClaw can efficiently solve multi-scale hydrodynamic flow problems on much larger domains than would typically be feasible for uniformly refined meshes. GeoClaw has been used for at least one dam failure problem previously and shown to produce results with good agreement with observational data (George, 2011). Inputs for GeoClaw are user-defined topography, reservoir parameterization (water surface elevation, boundary), dam failure specifications (height, location, timing), and a roughness parameter. One of the chief contributions of this study is to provide more evidence that GeoClaw should be considered further for dam failure modeling.

2.3 Previous Work

Researchers have developed a wide range of computational models for dam failure. Below, we describe computational models of the Teton Dam and Malpasset dam failures.

Table 1. Comparison of GeoClaw Software to HEC-RAS software, focus on components integral to dam failure numerical modeling such as numerical schemes, mesh shape, and adaptive refinement capabilities (Clawpack Development Team, 2020; Berger et al., 2011; Arcos & LeVeque, 2015; Brunner, 2002, 2016). Key differences accounted for in this study include the numerical schemes, interactive GUI, and mesh parameterization.

Characteristic	GeoClaw	HEC-RAS
Developer	Univ. of Washington	U.S. Army Corps Engineers
Adaptive Mesh Refinement	Yes	No
Discretization	Explicit FV	Implicit/Explicit FV
Shock-Capturing	Yes	Yes
1D/2D Linkages	No	Yes
Parallel Capabilities	Yes	Yes
Mesh Shape	Cartesian	Poly. Cells, User-Defined
Interactive GUI Interface?	No	Yes
Variable Manning's Roughness	Yes	Yes

2.3.1 Teton Dam Failure

2.3.1.1 *Bureau of Reclamation 1977* Reclamation used a preliminary version of HEC-RAS, called USTFLO (Gradually Varied Unsteady Flow Profiles model) to investigate the Teton Dam failure (Land, 1980). Reclamation used a 1D model with horizontal water surface traverse to the flow to model the failure (Gundlach & Thomas, 1977). The model was parameterized with an instantaneous flood development sequence and full dynamic routing to perform breach analyses (Land, 1980). The 1976 Reclamation data sets (Table 2) can be compared with USTFLO Reclamation 1977 study results at Gundlach and Thomas (1977).

2.3.1.2 *Balloffet and Scheffler 1982* Balloffet and Scheffler applied a 1D finite-difference (FD) model to simulate the Teton Dam failure flood in an explicit scheme ((1982)). This study used a network of channels and reservoirs, considering the progression inundation and drying of the floodplain, to model the flood. Their results indicate that a 1D-FD model using the network analysis allows for a more accurate representation of flood

Table 2. Historical data for downstream locations with corresponding flood depth, arrival times (5 June 1976), and distance from the dam; sourced from historical records (Reclamation, 1976; USGS, 1976).

Location	Distance [1]	Arrival Time [2]	Peak Flow	Max. Depth [3]
Teton Canyon	4 km	12:05	65,129 m ³ /s	15 m
Teton Canyon Mouth	8 km	12:10-12:20	X	12 m
Wilford	13.5 km	12:45	X	4 m
Teton Town	12.9 km	12:30	30,016 m ³ /s	3 m
Sugar City	19.8 km	13:30	X	3 m
Rexburg	24.6 km	14:30	X	2.5 m

(1) where 'distance' refers to the distance from the dam to the historical observation location (2) where 'arrival time' refers to the flood wave arrival time on 5 June 1976 in 24-HR clock time (3) where 'max. depth' refers to the maximum flood wave depth in the historical observation location

223 propagation than the methods of previous studies, which used 1D models producing av-
224 eraged stage and discharge across the floodplain (Gundlach & Thomas, 1977).

225 2.3.1.3 *Idaho National Laboratory 2015* Idaho National Laboratory (INL), Boise
226 State University, and Neutrino Dynamics Inc. modeled a hypothetical and exaggerated
227 Teton Dam failure. The study parameterized the Teton Dam breach with a Teton Reser-
228 voir WSE of 115 m, compared to the historical 82 m WSE (Reclamation, 2000). The sce-
229 nario models an exaggerated Teton Dam Failure and the resulting inundation of a fic-
230 titious nuclear power plant. The inundation at INL was modeled using 3D Smoothed Par-
231 ticle Hydrodynamics (SPH) - a robust Lagrangian approach for simulating fluid flows.
232 The breach was exaggerated to show a dramatic coupling of the flood (Smith et al., 2015).
233 This coupling effort was modeled in three stages: (1) 2D GeoClaw simulation, (2) 3D
234 domain of Neutrino Flow, and (3) Inflow to the 3D domain. The GeoClaw computational
235 model used an instantaneous dam failure with a vertical wall of water where the dam
236 was located at an initial water height of 115 m from ground level (Smith et al., 2015).
237 The GeoClaw results were one-way coupled to the 2D DualSPHysics SPH open-source
238 code coupled with the 3D SPH area (Smith et al., 2015). This work served as a prelim-
239 inary test case for the GeoClaw software in modeling the Teton Dam failure.

240 2.3.2 *Malpasset Dam failure*

241 2.3.2.1 *GeoClaw study* The GeoClaw study of Malpasset Dam failure by George
242 was the first to apply GeoClaw to dam failure modeling (George, 2011). The prelimi-
243 nary results for the first validation of this code for dam-break flooding problems demon-
244 strated that GeoClaw is a viable alternative to using specially developed unstructured
245 meshes exhibiting minimal computational cost with result accuracy because of AMR's
246 efficiency (George, 2011). This study compared GeoClaw results to results of the com-
247 mercial software package TELEMAC-2D (Valiani et al., 2002; Hervouet & Petitjean, 1999).
248 The comparison concluded that all three numerical simulations had nearly identical re-
249 sults that differed more from laboratory data than from one another (George, 2011).

250 2.3.2.2 *HEC-RAS study* HEC-RAS v4.1.0 was used to model the Malpasset dam
251 breach benchmark problem compared to 2D modeling software Flood Modeller (formally
252 known as ISIS) (Almassri, 2011). In simulating the dam break test, HEC-RAS produced
253 results similar to the historical numerical values. The study concluded that HEC-RAS
254 was efficient, fast, and accurate for simulating dam breaches. However, both Flood Mod-
255 eller and HEC-RAS models required a sizable amount of data input to initiate the mod-
256 els and produce reliable results (Almassri, 2011).

257 3 Methods and Data

258 3.1 Metadata and Domain

259 This study parameterizes the dam geometry, reservoir, and domain as inputs for
260 the numerical simulations. We use a large domain, the Teton Dam study area (88.5 km
261 x 43.5 km), to evaluate the performance of a uniform Manning's n (surface roughness
262 coefficient) and the software's handling of the complex terrain-the steep-walled narrow
263 canyon and the floodplain. This study selected a downstream limit of the model at 54 km,
264 or just past the town of Roberts, Idaho (US). This study chose the downstream limit based
265 on the limitation of high-resolution topographic data. However, this limitation does not
266 prevent us from a complete study comparing the GeoClaw and HEC-RAS models. In
267 HEC-RAS we also parameterize the earthen dam piping failure to appropriately simu-
268 late the time-dependent failure sensitivity analysis.

269 For this benchmark problem parameterization, horizontal and vertical datum con-
270 verations were used to align topographic features with historical values. Two topographies

were implemented in this modeling effort, originally sourced from the USGS in projection WGS 84 (USGS, 2015): "TetonLarge" (6.99 KB) at 30 m resolution and "TetonHighRes" (7.77 KB) at 10 m resolution. TetonHighRes and TetonLarge form a 88.51 x 43.45 km³ domain. The joined topography was used in the GeoClaw and HEC-RAS models to enable model comparison.

276 3.2 Reservoir volume

This study estimated the initial reservoir volume using historical design drawings and updated volume estimates to approximate the reservoir extent (Reclamation, 1976; Reclamation, 2000). Three reports by Reclamation provide three different estimates of the reservoir volumes at time of failure: $3.08 \times 10^8 \text{ m}^3$ - (1976), $2.89 \times 10^8 \text{ m}^3$ - (2000), and $3.10 \times 10^8 \text{ m}^3$ - (2008). The values seem similar but may be significant in downstream inundation depths; this study tests the model's sensitivity to the reservoir volume. Each of these calculations was conducted differently. Balloffett and Scheffler (1982) suggest that the (1976) Reclamation's initial reservoir volume was calculated using an elevation-storage curve, implying a horizontal reservoir surface which additional work determined to not significantly affect 1D flood routing (Thomas, 1977; Fread, 1977; Reclamation, 1976). In comparison, Reclamation improved volume estimates in (2000) by using higher resolution contour maps to calculate volume from contour elevation maps.

These volume estimates were checked using Google Earth using the historical parameters for the reservoir to map the quasi-prismatic river channel in sections. Spero et al. calculated the average height, and got an upper bound estimate of $3.51 \times 10^8 \text{ m}^3$ (Spero & Calhoun, 2020). The volume discrepancies show the necessity for this study to determine the influence of reservoir volume on downstream flow using the 2D HEC-RAS software and sensitivity analysis. The Teton Dam reservoir elevation was parameterized at an initial elevation of 1617 m.

296 3.3 GeoClaw Simulation

The first step in constructing the GeoClaw simulation involved determining key input parameters and creating the reservoir. For the GeoClaw model, this study uses values from Reclamation because of their datum and more accurate volume calculation method (2000). To parameterize the reservoir, a polygon was defined at Teton Canyon's edges, extending 16 km upstream from the dam site. The GeoClaw 'reservoir' polygon was used to estimate the volume and flow. Points were plotted at the historic dam height throughout the reservoir – 1624 m MSL. Then, the Teton River for was filled with water to 1617 m water surface elevation (NAVD 88) (Reclamation, 2000). The reservoir volume in GeoClaw was $3.05 \times 10^8 \text{ m}^3$, considered to be within suitable range.

GeoClaw was parameterized using an instantaneous dam breach assumption; the first time step of the simulation represents the dam's immediate removal. We also enforced refinement by associating minimum flow criteria with maximum mesh resolution, ensuring the reservoir was refined enough to provide reasonable resolution to capture the moving flood front. The Manning's coefficient for the study area was set to be a constant of 0.06. This value was estimated from a field inspection of the floodplain and Teton River Canyon. For confirmation of the Manning's n value, we used Manning's n definitions (Chow, 1959), gauge data, high watermark data, field interviews, newspaper records, high water marks, and hydrograph comparisons, and verification data to determine the confidence of 0.06 value (Gundlach & Thomas, 1977).

Both stationary and Lagrangian gauges were inserted into the GeoClaw simulation, tracking flood wave arrival time and depth downstream. Stationary gauges output the SWE solution at fixed geographical positions and serve as proxies for comparison with

Table 3. Stationary Gauge Locations in GeoClaw Teton Dam domain.

Gauge Name	Latitude	Longitude
Teton Canyon	-111.5939	43.9341
Teton Canyon Mouth	-111.6664	43.9338
Wilford	-111.6721	43.9144
Sugar City	-111.7601	43.8633
Rexburg	-111.7923	43.8231

319 historical records and accounts and log the flood wave arrival times and peak flow val-
320 ues.

321 To visualize the flow field, we create a series of output images (.png files), viewed
322 in the Google Earth browser. The color scale on the images is used to depict inundation
323 depth.

324 Tracking the fluid continuum downstream was difficult around localized topographic
325 highs (ex: Menan Butte 1713 m), so this study used two 3 x 3 grids of Lagrangian par-
326 ticles (Supplementary Files; Table 1). Our study is the first to use Lagrangian gauges
327 in GeoClaw for terrestrial flow modeling. The trajectories of the Lagrangian particles
328 demonstrate the fixed velocity at points in space, an Eulerian representation of the flow.
329 The passively advected tracer particles move according to interpolated Eulerian veloc-
330 ity fields. We visualize the particles on top of water particles through (1) the Fundamen-
331 tal Principle of Kinematics (the velocity at a given position and time is equal to the ve-
332 locity of the parcel that occupies that position at that time), (2) The material or sub-
333 stantial derivative relates the time rate of change observed following a moving parcel to
334 the time rate of change observed at a fixed position; where the advective rate of change
335 is in field coordinates. 3) To assert the conservation laws for volume and momentum within
336 an Eulerian system, we need to transform the time derivative of an integral over a mov-
337 ing fluid volume into field coordinates; this leads to or requires the Reynolds Transport
338 Theorem (Price, 2004). More information for the GeoClaw particles is available at (Clawpack
339 Development Team, 2021a).

340 3.4 HEC-RAS Simulation

341 The first step to parameterizing the historic Teton Reservoir was developing a ter-
342 rain data set in the HEC-RAS RAS Mapper. The projection was set to the new raster
343 projection for unit agreement using ArcGIS Pro 10.8.1 (US customary units were used
344 within the HEC-RAS model). The projection file was created with ArcGIS Pro 10.8.1.
345 A new terrain was data set was created by layering TetonHighRes (10 m) on TetonLarge
346 (30 m). TetonHighRes topography has a finer resolution, so it was given a higher prior-
347 ity in the combined Terrain Layer. To develop the 2D computational mesh, a polygon
348 boundary was drawn for the 2D Teton Reservoir area. The Teton Reservoir (denoted TDRES2D)
349 nominal grid resolution of 61 times 61 m cells was used to build the HEC-RAS compu-
350 tational mesh.

351 Similarly, the 2D downstream flow area was constructed using the RAS Mapper
352 geometry editor. The 2D downstream flow area was refined with each run to reflect the
353 computational area where flow occurred, improving computational efficiency. The final
354 2D downstream flow area for both the instantaneous HEC-RAS and the time-dependent
355 HEC-RAS models used a uniform Manning's coefficient of 0.06. The sensitivity analy-
356 sis for this study focuses on the importance of Manning's coefficient. The base of the down-
357 stream flow area (2D-DSTREAM) fed into a boundary condition line (BC Line) where

358 the water could exit the simulation. Additionally, two break-lines were inserted into the
 359 simulation to force a cell edge at two important lateral features, differences in elevation.
 360 Through break-lines, we are better able to simulate water flow over cells. The first break-
 361 line was within the Teton Dam canyon downstream of the Teton Dam. Break-line 2 was
 362 inserted approximately from (43.98, -111.58) to (43.90, -111.65).

363 The two 2D Flow Area elements (TD-RES-2D and TD-DSTREAM) are connected
 364 with a storage area 2D connector (SA/2D), which formed the dam as a weir or embank-
 365 ment. The dam was parameterized in the geometry editor for the instantaneous dam fail-
 366 ure by modeling the weir to fit the terrain. The time-dependent dam failure was also pa-
 367 rameterized in the geometry editor. The dam structure was built using the historic dam
 368 height of 1626 m (NAVD 88) (Reclamation, 1976).

369 Historical values were implemented to match historical literature values and fit the
 370 terrain using the Breach (plan data) section of the SA/2D connector. The best fit was
 371 identified as having a Center Station of 284 m, a final bottom width of 55 m, and a fi-
 372 nal bottom elevation of 1549 m (NAVD 88). For additional time-dependent dam failure
 373 parameterization, the piping coefficient was 0.5 based on Reclamation (1976), and the
 374 initial piping elevation from historical literature (first spot of seepage) was 1597 m (Reclamation,
 375 1976). The start date and time of the failure to achieve a maximum breach at 11:57 were
 376 and a simulation start time of 11:00; start time was chosen based on time stamps on pho-
 377 tographs from 1976 failure. A sine wave breach progression was used as the breach pro-
 378 gression method, validated in other literature studies bhandari2017one. The progression
 379 method depicts how the breach grows from initiation to maximum size during the breach
 380 period (bp), where for this study, the bp is 11:00-12:00, one hour. The sine wave pro-
 381 gression speed varies over the development time according to the first quarter cycle of
 382 a sine wave. It was chosen as it most closely resembles an earthen dam breach (Ackerman
 383 et al., 2008; Yochum et al., 2008).

384 For the instantaneous dam failure plan, the simulation time starts at the time of
 385 breach, 11:57 on 5 June 1976 (Reclamation, 1976) and runs for simulated time 12 hours
 386 and 43 minutes (24:00 6 June 1976). The computational interval and time stepping scheme
 387 depends on the Courant–Friedrichs–Lewy condition (CFL). Besides the geometry files,
 388 the primary difference in the two analysis runs was the simulation start times. The time-
 389 dependent dam failure required the sine wave initiation and the breach lasted 1 hour,
 390 the simulation begins before the dam breach (11:00) and runs until 24:00 6 June, 1976.
 391 Additionally, the first HEC-RAS model was constructed using the Diffusion Wave equa-
 392 tions. Then, once the model was stable, this study changed the model to solve using the
 393 Full Momentum SWE equations.

394 4 Results of GeoClaw and HEC-RAS Models

395 Results are presented in three sections. Section 4.1 focuses on stationary gauge re-
 396 sults beginning upstream at the Teton Dam site and moving downstream until Rexburg
 397 (25 km downstream; Table 3). Section 4.2 focuses on the lateral extent of flooding. Sec-
 398 tion 4.3 focuses on Lagrangian gauge components in GeoClaw and results.

399 4.1 GeoClaw and HEC-RAS Instantaneous Dam Failure Results

400 We compare all historic inundation depths (maximum) against numerical simula-
 401 tions performed using our GeoClaw numerical dam model. The results focus on five of
 402 the GeoClaw and HEC-RAS stationary gauges, which logged historic arrival times (hrs)
 403 and maximum flow depth (m) of the flood during the model’s simulation time.. The gauge
 404 results are presented below in sequential order moving from the dam progressively down-
 405 stream: (i) Teton Dam Canyon gauge, (ii) Teton Dam Canyon Mouth gauge, (iii) Wil-
 406 ford gauge, (iv) Sugar City gauge, and the (v) Rexburg gauge. The sensitivity analy-

407 ses use results from three profile lines that logged flow and flood wave arrival times: (a)
 408 Sugar City, (b) Rexburg, and (c) Menan Butte Butte (Table 3).

409 ***4.1.1 Teton Dam Canyon Gauge***

410 The GeoClaw Teton Dam Canyon gauge showed a 7.6 m maximum depth flood wave,
 411 averaging to 7.3 m, propagating down the canyon. As GeoClaw models an instantaneous
 412 dam breach, the inundation flood wave arrival time for the GeoClaw Teton Dam Canyon
 413 gauge occurs during the second time step – almost immediately at 12:05. In compari-
 414 son, photographs at the time of failure at the location of the GeoClaw Teton Dam Canyon
 415 gauge demonstrate a maximum flood wave depth of about 15 m and arrival times at 12:05
 416 (Reclamation, 1976). The HEC-RAS Teton Dam Canyon Gauge shows 41.3 m maximum
 417 depth flood wave, within the Teton Canyon. The flood wave arrives at the HEC-RAS
 418 gauge at 11:59, just two minutes following the instantaneous dam breach at 11:57 (Reclamation,
 419 1976).

420 ***4.1.2 Teton Dam Canyon Mouth Gauge***

421 Next downstream, the GeoClaw Teton Dam Canyon Mouth gauge records flood wave
 422 arrival time five minutes later at 12:10. The GeoClaw gauge registers a maximum flood
 423 wave depth of 2.1 m inundation, not agreeing with historical values of 11.8 m-12.2 m (Reclamation,
 424 1976). Then, as the flood laterally spread out of the canyon, it does not flood the town
 425 of Teton, agreeing with the lateral extent of the historic flood. However, the historic depths
 426 are greater than those modeled in GeoClaw by 9.2 m. For the HEC-RAS Teton Dam Canyon
 427 Mouth Gauge, the maximum recorded depth was 20.6 m, 8.5 m greater than historical
 428 values (Reclamation, 1976). The HEC-RAS gauge logged a flood wave arrival time of
 429 12:06.

430 ***4.1.3 Wilford Gauge***

431 At 12:38, when the wave is progressing downstream, the GeoClaw Wilford gauge
 432 displays a depth of 2.7 m. Historical literature values show flood waves reaching Wilford
 433 at approximately 12:45 with 3.1 –4.6 m inundation depth (Reclamation, 1976). The HEC-
 434 RAS model Wilford gauge displays maximum inundation depth of 7.2 m overestimating
 435 the 3.1 –4.6 m in historical data by about 2.6 meter. Additionally, HEC-RAS had an ar-
 436 rival time at 12:34.

437 ***4.1.4 Sugar City Gauge***

438 The GeoClaw Sugar City gauge showed a flood wave arrival time at 13:05. The his-
 439 torical literature value for arrival time was 13:30, and flood depth was 3.1 m (Reclamation,
 440 1976). The depth, as displayed in the GeoClaw gauge, is 1.2 m. The HEC-RAS Sugar
 441 City gauge registered a flood wave arrival time at 14:05 (Reclamation, 1976) and a max-
 442 imum depth of 3.4 m.

443 ***4.1.5 Rexburg Gauge***

444 The GeoClaw Rexburg gauge demonstrated model values between 1.2 –1.5 m; his-
 445 torical depths were 2.4 m(Reclamation, 1976). The Rexburg GeoClaw gauge logs an ar-
 446 rival time at 14:30, and the historic arrival time is 14:30 (Reclamation, 1976). The HEC-
 447 RAS Rexburg gauge shows an arrival time of 16:25, an hour and 55 minute difference
 448 from historical values. The gauge also logs a maximum depth of 34 m.

449 ***4.1.6 Lateral Extent of Modeled Floods and Computational Costs***

450 The other evaluation principle for the comparison criterion for GeoClaw was de-
 451 termining the lateral flood extent. The GeoClaw model showcased a flood area covered
 452 313 km^2 which is within $\pm 80 \text{ km}^2$ of the historic inundation extent of 337 km^2 for the
 453 time simulated (Reclamation, 1976). In comparison, the HEC-RAS model demonstrated
 454 a flood area of 451 km^2 , which is also within $\pm 80 \text{ km}^2$ of the historical 337 km^2 (Reclamation,
 455 1976).

456 GeoClaw computational time for runs on the R2 compute cluster, installed at Boise
 457 State University, is 17 minutes processing time and 15 minutes for plotting. For HEC-
 458 RAS the base model run time was 31 minutes, which includes both run and plot time.
 459 Therefore, GeoClaw and HEC-RAS have similar computational wall clock times, 32 min-
 460 utes compared with 31 minutes. The GeoClaw model ran on 16 OpenMP threads on a
 461 single node of the R2 super compute cluster (Boise State Research Computing, 2017).
 462 The computational budget of the HEC-RAS Teton Dam base model included 28 cores
 463 and 28 threads on one node. HEC-RAS used a desktop for runs; Intel Xeon E5-2680 v4
 464 14 core 2.4GHz (x2).

465 ***4.1.7 Lagrangian Gauges Results***

466 This study introduced Lagrangian particles into our depth-averaged flow field to
 467 better image the downstream flows for indicating turbulence. Results indicated swirling
 468 flow dynamics were observed in the dam failure simulation behind the local topographic
 469 high of the domain, Menan Butte (elevation 1713 MSL). As the Lagrangian gauges up-
 470 dated at each time step interval, both clusters demonstrated interesting flow paths within
 471 the downstream flood (Supplementary Files; Video 1). For example, eddying occurred
 472 upstream of Menan Butte and detained six of nine Lagrangian gauges for over 15 min-
 473 utes. Menan Butte is a large topographic feature, and thus results showed the flow was
 474 substantially affected below the Henry's Fork river, where the Snake River begins in East-
 475 ern Idaho. At Henry's Fork, this study noted increased velocities for particles that in-
 476 teracted with the river, as they moved further downstream per time-step than other par-
 477 ticles from the same cluster moving over the farmland domain.

478 ***4.2 HEC-RAS Sensitivity Analysis***

479 This study used four sensitivity analyses to evaluate which parameters in the HEC-
 480 RAS model control the numerical solutions (Table 3). For the HEC-RAS model results,
 481 we analyzed the output flow hydrograph head and tailwaters, the computation log for
 482 error percentage, the gauge features for water surface elevation, and three profile lines
 483 for flow. The three profile lines, Sugar City, Rexburg, and Menan Butte were chosen based
 484 on relative distance downstream and the plethora of historical data. Table 3 summarizes
 485 the four sensitivity analyses:

- 486 1. Manning's roughness coefficient
- 487 2. Volume Analysis
- 488 3. Instantaneous and Time-Dependent Dam Failure
- 489 4. Characteristic Size of the Computational Mesh

490 Critical trends in the results demonstrate that the reservoir volume controls the
 491 peak flow but not the peak flow arrival time. In contrast, the computational mesh con-
 492 trolled peak flow arrival time but had similar peak flows. The Manning's n value was
 493 likely overestimated in this study at 0.06, exhibited in the Manning's sensitivity study.
 494 Lastly, the instantaneous dam breach assumption was validated as the base model val-
 495 ues were identical in peak flow arrival time and comparable in peak flow.

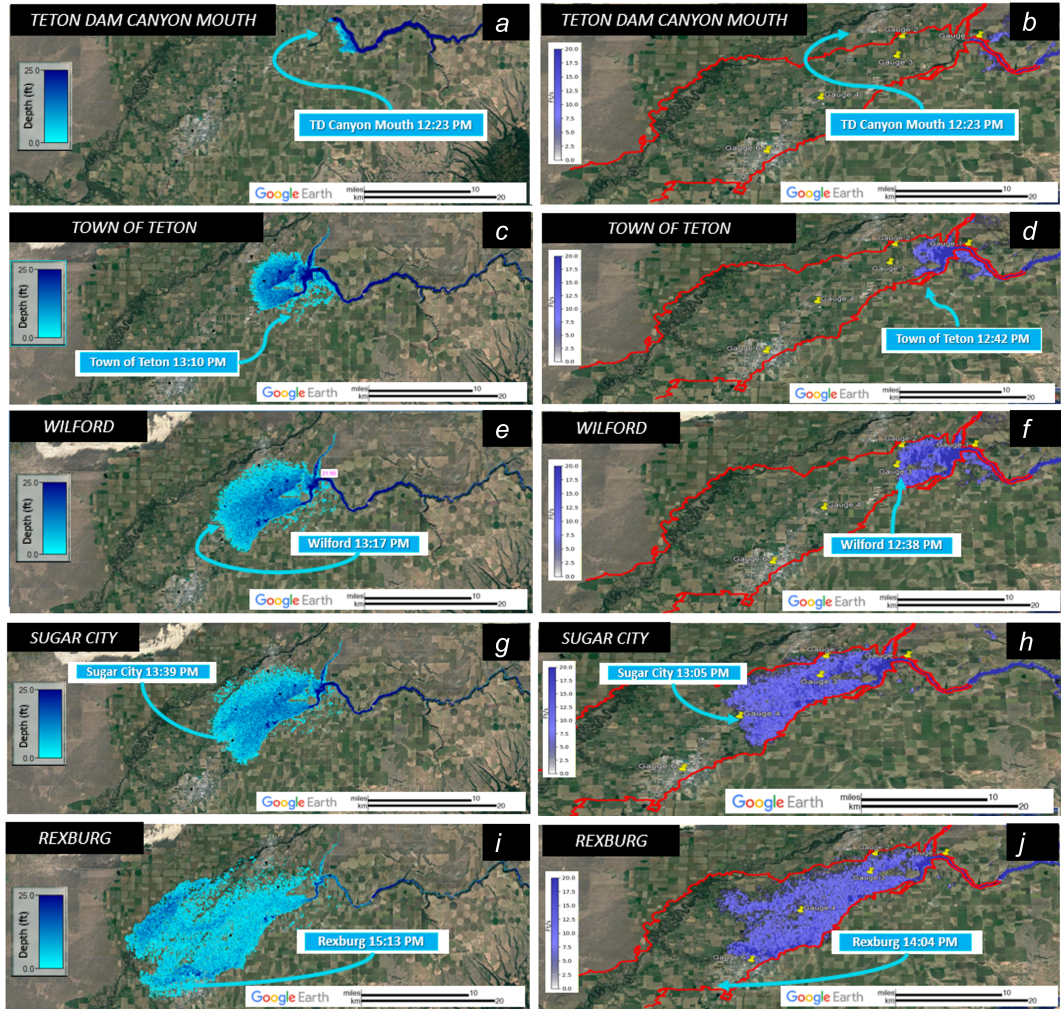


Figure 1. GeoClaw results compared with historical data and HEC-RAS results; focused on lateral extent of the flood (blue). The red outline denotes the extent of the historical flood from (USGS, 1976), and the yellow pushpins in the GeoClaw model results show the specific gauge locations; latitudes and longitudes of the gauges can be found in Table 3. Figures a-e move progressively downstream from the dam, and a,c-e are gauges used in model comparison.

4.2.1 Manning's Roughness Coefficient Sensitivity Analysis

The Manning's n analysis compared roughness values of 0.03-0.07 to determine if the Manning's n value controlled the numerical solution. The base model used a value of 0.06, and all Manning's n values had a slightly different mesh than other models with an expanded domain laterally to allow for natural flow instead of mesh-directed flow. At the Sugar City profile line, the 0.03 Manning's model peak flow arrived first at 13:18, followed sequentially by progressively smaller Manning's (0.04, 0.05, 0.06, and 0.07). The peak flow was largest at the Manning's 0.03 model ($35,300 \text{ m}^3/\text{s}$) and smallest for the Manning's 0.07 model ($22,000 \text{ m}^3/\text{s}$). At the Rexburg profile line, these trends continued as the Manning's 0.03 model peak flow arrived first (14:41), and the Manning's 0.07 model peak flow arrived last (16:25) – a difference of 1 hour and 45 minutes. Historically, the wave arrived in Rexburg at 14:40 (Reclamation, 1976). The peak flow at the Rexburg profile line was largest for the Manning's 0.03 model ($21,800 \text{ m}^3/\text{s}$) and lowest for the Manning's 0.07 model ($12,500 \text{ m}^3/\text{s}$). The 0.06 Manning's n model (this study's base model) arrived at 16:25 with a flow of $14,000 \text{ m}^3/\text{s}$. Further downstream, at the Menan Butte profile line, the Manning's 0.03 model peak flow arrives 16:07, and the Manning's 0.07 model peak flow arrives 19:01. The Manning's 0.03 model peak flow was observed as $7900 \text{ m}^3/\text{s}$, whereas the Manning's 0.07 was recorded as $4000 \text{ m}^3/\text{s}$. The base model, Manning's 0.06, recorded $4600 \text{ m}^3/\text{s}$ at 19:01. The peak flow between the largest (0.07) and the smallest (0.03) Manning's n models differ by about 23%.

4.2.2 Volume Sensitivity Analysis

The volume sensitivity analysis compared two volumes. Volume 1 was a volume of $2.29 \times 10^8 \text{ m}^3$ volume (235,978 acre-ft) representing the historical Reclamation volume value (Reclamation, 2000). Volume 2 was the volume created using the initial reservoir depth of 617 m water surface elevation (WSE; NAVD 88) $2.63 \times 10^8 \text{ m}^3$ volume (213,294 acre-ft model, HEC-RAS Base Model). For the first profile line, Sugar City, the base model ($617 \text{ m}^3/\text{s}$) arrived at 14:05, similar to the historic volume model (13:58). The peak flow at Sugar City between the two models differs by $3200 \text{ m}^3/\text{s}$; historic volume model flow of $27,600 \text{ m}^3/\text{s}$ and base model flow of $24,400 \text{ m}^3/\text{s}$. Further downstream at the Rexburg profile line, the base model arrived at 16:25, and the historic volume model arrived at 16:13. The peak flow rates differed by $2400 \text{ m}^3/\text{s}$, with the historic volume model logging the higher flow at $16,400 \text{ m}^3/\text{s}$. Then, at the third profile line, Menan Butte, the volume analysis demonstrated the historic volume model to arrive first at 18:38, and then the base model arrived at 19:01, a difference of fewer than 25 minutes. The peak flow rate for the models were comparable, with $4600 \text{ m}^3/\text{s}$ (base model) and $5300 \text{ m}^3/\text{s}$ (historic model), which differ by about $674 \text{ m}^3/\text{s}$.

The peak flow differs between the historic volume model (Volume 1) and Volume 2 by 6% at the Sugar City profile line, 8% at the Rexburg profile line, and 7% at the Menan Butte profile line. The flood wave arrival times differ by about 0.4% at the Sugar City profile line, 0.6% at the Rexburg profile line, and 1% at the Menan Butte profile line.

4.2.3 Characteristic Size of Computational Mesh Analysis

The results of the computational mesh analysis compare the base model mesh (242,210 cells; $274 \times 274 \text{ m}$ - base model mesh) to a mesh with cell sizes increased by 50% (11,157 cells; $411 \times 411 \text{ m}$ - lower resolution mesh [LRM]) and a mesh with cell sizes decreased by 50% (980,030 cells; $137 \times 137 \text{ m}$ -higher resolution mesh [HRM]). The computational cost for the HRM was 4:20:15 hours (15,615 seconds), in comparison to the LRM, which processed in 14:03 minutes (843 seconds). The base model computes at 31:13 minutes (1873 seconds). The HRM runs 52% slower than the base model cost, a significant increase in cost.

Table 4. HEC-RAS Sensitivity Analyses including the (i) Manning's n models, the (ii) reservoir volume models, the (iii) Characteristic Mesh Size models, and the (iv) instantaneous and time-dependent dam breach models. Table includes historic values to reference, sourced from (USGS, 1976; Reclamation, 1976; USGS, 2021).

HEC-RAS Sensitivity Analysis						
	Sugar City profile Line	Resburg Profile Line	Menan Butte Line	Flow (cubic m)	Arrival Time (hh:mm)	Flow (cubic m)
Historical Values				30,016 m ³	13:30	None
Manning's n	0.03 0.04 0.05 0.06 0.07	35.458 30.957 27.366 24.488 27.745		13:18 13:34 13:50 14:05 14:20	21,836 18,517 16,005 14,046 12,485	14:41 15:16 15:51 16:25 17:00
Reservoir Volume	2.29 × 10 ⁸ m ³ Model 2.63 × 10 ⁸ m ³ Model	24,488 24,488		14:05 14:05	14,046 14,046	16:25 16:25
Computational Mesh Cell Size	Base Model Cell Size 50% Incr. Cell Size 50% Decr. Instantaneous Time-Dependent	24,488 22,979 22,968 24,488 24,488		14:05 14:14 14:14 14:05 14:05	14,046 11,111 11,106 14,046 14,046	16:25 17:04 17:04 16:25 16:25
Dam Failure Mode						4611 4611 3963 4611 4611
						19:01 19:01 20:20 19:01 19:01

544 For the profile line results, the LRM and HRM produced similar results. At the
 545 Sugar City profile line the LRM registered $22,858 \text{ m}^3/\text{s}$ compared to the HRM $22,800 \text{ m}^3/\text{s}$;
 546 a difference of 0.1% with both flows lower than the base model flow of $24,400 \text{ m}^3/\text{s}$, but
 547 only by 3%. At the Sugar City Profile line then, the base model arrives first at 14:05,
 548 followed by the LRM and HRM arriving both at 14:14. Both the HRM and LRM log
 549 a flow of $11,100 \text{ m}^3/\text{s}$, whereas the base model's flow was 11% higher at $14,000 \text{ m}^3/\text{s}$. The
 550 arrival time of the HRM and LRM were both 17:04, and the base model was 16:25. Fur-
 551 ther downstream at the Menan Butte profile line, the LRM and HRM arrive again si-
 552 multaneously (20:20) after the base model (19:01). The LRM and HRM flows were within
 553 1 m^3/s being $4000 \text{ m}^3/\text{s}$ respectively); 6% below the base model flow estimate of $4600 \text{ m}^3/\text{s}$.

554 4.2.4 Instantaneous and Time-Dependent Dam Breach Model Results

555 For instantaneous breach model versus time-dependent breach model sensitivity
 556 analysis, this study assesses the time-dependent scenario and the instantaneous dam breach
 557 scenarios in HEC-RAS. Processed flood wave arrival times accounted for the time-dependent
 558 breach start time of 10:00 differing by 1:57 hours from the instantaneous breach. At Sugar
 559 City profile line, the instantaneous dam breach logs a flow of $24,400 \text{ m}^3/\text{s}$ compared to
 560 the time-dependent dam breach value of $243,400 \text{ m}^3/\text{s}$ a difference of 0.2%; both arrive
 561 at 14:05. At the Rexburg profile line, both models arrive at 16:25 and log extremely sim-
 562 ilar values (time-dependent model: $14,000 \text{ m}^3/\text{s}$, instantaneous model: $14,000 \text{ m}^3/\text{s}$). Then,
 563 at the Menan Butte profile line, both models arrive at 19:01 and log similar flow values.
 564 The time-dependent breach logged and the instantaneous breach both logged $4600 \text{ m}/\text{s}$
 565 logged $4600 \text{ m}^3/\text{s}$. Furthermore, both computational costs were similar varying only by
 566 30 ± 2 minutes.

567 5 Discussion

568 Dams in the US are aging, and the frequency of dam failures increases with age.
 569 Floods are one of the most frequent and costly natural disasters the US faces – includ-
 570 ing dam failures flooding (ASDSO, 2021). Dam failures pose a significant threat to hu-
 571 man life downstream of the dam. One must first validate and benchmark the software
 572 using a historical dam failure assessment to forecast dam failures. One of the guiding
 573 questions of the study focused on evaluating GeoClaw for dam failure downstream mod-
 574 eling. The evaluation was based on mathematical formulation controlling flood move-
 575 ment, the capability to predict inundation extent and final flow depth through a numer-
 576 ical method, and the ease of use, performance characteristics, and tools for visualization
 577 and post-processing. The second guiding question investigated the model's sensitivity
 578 to its parameterization and uncertainty.

579 The stationary gauges used in the two models, HEC-RAS and GeoClaw, allow com-
 580 parison of flood wave depth and flood wave arrival time. This section discusses the first
 581 two gauges: Teton Dam Canyon gauge, Teton Dam Canyon Mouth gauge, and the Wil-
 582 ford gauge. The first gauge, Teton Dam Canyon, showed a flood wave arrival time at 12:05
 583 as 7.6 m depth. We consider the GeoClaw Teton Dam Canyon gauge to agree with his-
 584 torical records when evaluating the flood wave arrival time (12:05 historical arrival time)
 585 (Reclamation, 1976), but not when evaluating by depth as it underestimates the depth
 586 by 7.62 m. The HEC-RAS model overestimates the flow depth by 5.18 m but agrees with
 587 the historical flood arrival time. The GeoClaw Teton Dam Canyon Mouth gauge under-
 588 estimates the flood depth by 9 m.

589 In contrast, the HEC-RAS model's Teton Dam Canyon Mouth gauge overestimates
 590 the depth by about 27 m, and the flood wave arrival time differs from historical records
 591 by over 30 minutes. These differences are significant, and the slow arrival time and over-
 592 estimation of the depth suggest that Manning's n value of 0.06 is too high in the canyon.
 593 However, it is important to note that the Teton Canyon presents the most challenging

portion of the flow to model using the SWE. As within the canyon, the extreme vertical accelerations are not well captured by the SWE model.

Continuing the discussion of gauge results with the Wilford, Sugar City, and Rexburg gauges, this study finds GeoClaw and HEC-RAS values similar to historical values. At the Wilford gauge, the GeoClaw model estimated the depth within 1.2 m of historical values and the flood arrival time within 15 minutes – which we consider to be excellent agreement. The HEC-RAS model overestimates the flood depth by 4.6 m and demonstrates a flood arrival time difference of 40 minutes which is significant (12:38 historical versus 13:17 model). The GeoClaw Sugar City gauge logged general agreement to the historical literature value arrival time (within 25 minutes) but underestimated the depth by 1.8 m. In contrast, the HEC-RAS gauge estimated the flood within 0.6 m of the historical value, and the flood arrival time is within 10 minutes – we consider the HEC-RAS Sugar City gauge to be in excellent agreement with historical data. Further downstream, the GeoClaw Rexburg gauge also demonstrates inundation agreements with model values within 0.9 m of historical values and the same model arrival time as historical arrival time (14:30). The HEC-RAS Rexburg gauge slightly overestimated historical data; the arrival time differs by over 30 minutes.

Major trends in the results show that the GeoClaw model demonstrates good agreement with historical values for inundation extent, although consistently underestimating depth values. The base model results for HEC-RAS showed agreement with both GeoClaw and with historical data, although consistently overestimating the maximum flow depth and arrival times. For lateral extent evaluation, the GeoClaw model was 313 km^2 which is within $\pm 77.7 \text{ km}^2$ of the historic inundation extent of 336.7 km^2 . However, the HEC-RAS model overestimated the extent which could be related to overestimating the WSE in the reservoir; 450 km^2 HEC-RAS base model compared to the 337 km^2 in historical archives, (Reclamation, 1976).

In the assessment of the computational cost, both models are comparable with wall clock times between 15–17 minutes. HEC-RAS post-processing requires no additional plotting, whereas GeoClaw requires about 15 minutes of extra processing to produce visualization output. Overall, the results allowed this study to answer the three guiding questions and come across ideas for future work.

5.0.1 Suitability of *GeoClaw*

This study investigated if the GeoClaw model was suitable for dam failure downstream modeling of the Teton Dam failure (objectives outlined in Section 1). We determined the suitability of the GeoClaw software based on its capability to resolve lateral inundation extent, flood front arrival times, and maximum flood depths. For GeoClaw and HEC-RAS, the calculated area for the lateral extent of the flood largely agrees with historical data. We evaluate the five inundated simulation domains and the modeled time of the six stationary gauges inserted into the GeoClaw simulation for gauge data interpretation. We consider the model in excellent agreement if it predicts the flood wave arrival time within 15 minutes of historical data. We consider the model in good agreement if it predicts the wave within 30 minutes of historical data. Three of the five GeoClaw gauges log flood wave arrival times within ± 7 minutes (Teton Canyon, Teton Canyon Mouth, Wilford -excellent agreement), and all five gauges demonstrate good agreement with historical arrival times. By contrast, the HEC-RAS base model shows three gauges in excellent agreement, one gauge in good agreement, and the Rexburg gauge predicting an arrival time two hours after the historic wave arrived (14:30 compared to 16:25).

For assessing maximum flood depths, this study considered a model in excellent agreement if the depth values were within 1.5 m of historical values. The GeoClaw model is in good agreement if values are within 3 m of historical values. These values also take into account uncertainties in the model, such as ambiguity as to locations where histor-

ical values were collected (Reclamation, 1976). For GeoClaw, two gauges (Wilford and Rexburg) demonstrate excellent agreement with historical data, and Sugar City demonstrates good agreement with historical values. For HEC-RAS, only Sugar City demonstrated excellent agreement, and Rexburg demonstrated good agreement. The Wilford gauge was overpredicted by HEC-RAS (7.2 m compared to the historic 4 m). The trends of GeoClaw show it consistently underestimates the maximum flood depths in the confined canyon area (by 7.6 – 9.1 m). However, as the modeled GeoClaw flood wave moves downstream out of the canyon, it largely agrees more with maximum flow depths, illustrating perhaps a resolution limitation of GeoClaw in the steep canyon terrain. Potentially, for both HEC-RAS and GeoClaw, using a different roughness coefficient in the canyon could lead to improved and more realistic maximum flow depths.

Other factors considered in model results encompass flood volume, mesh refinement, code efficiency, and pre-processing and post-processing workflows. The pre-processing workflow for GeoClaw involved retrieving metadata in ASCII format and transferring that to the Boise State Compute Cluster R2 (Boise State Research Computing, 2017). In contrast, HEC-RAS topography processing required changing ASCII data to raster using ArcMap and ArcGIS Pro. When considering mesh refinement, GeoClaw's AMR is advantageous, only resolving where the flood propagates and not requiring an iterative approach to refining the user-defined mesh to improve the downstream mesh. For code and run time efficiency, HEC-RAS and GeoClaw have similar run times. With semi-parallel processing, GeoClaw could improve run times to similar processing and plotting speeds. For example, future work could use the ForestClaw package which could run GeoClaw using distributed computing (Calhoun & Burstedde, 2017). For the HEC-RAS post-processing workflow, as the model runs, the RAS Mapper window simultaneously updates and stores all results allowing for visualization over the terrain or online map imagery.

5.0.2 *What is the importance of breach progression in dam failure modeling?*

The importance of a dam breach was assessed by comparing the HEC-RAS time-dependent breach model to the instantaneous breach model. Both models yielded extremely similar results, and the same flood wave arrival times at all three profile lines. The sensitivity analysis required almost identical flows. Therefore, with the similar outputs between the two models, we consider using an instantaneous dam breach estimate rather than parameterizing the historical time-dependent dam breach to be valid.

5.0.3 *What is the uncertainty associated with using HEC-RAS for dam failure modeling?*

Another objective of this study was to determine the sensitivity of the HEC-RAS model. The results from the sensitivity analyses indicate the volume and the Manning's roughness coefficient were shown to largely control the solution and introduce uncertainty into the model.

For the volume sensitivity analyses, this study compared the historic volume of $2.29 \times 10^8 \text{ m}^3$ (Reclamation, 2000) to the base model volume of $2.63 \times 10^8 \text{ m}^3$. The results indicated that the peak flow values between the historic and base models were progressively aligned as the flood wave moved downstream and laterally expanded. From Sugar City (flow difference of $3200 \text{ m}^3/\text{s}$) to Menan Butte (difference of only $2400 \text{ m}^3/\text{s}$). However, the peak flow rates did show a range, so knowing an accurate reservoir volume is critical to building a reliable dam failure model.

In this study, the Manning's n value also controlled the solution. For instance, the Sugar City profile line logs the 0.04 n flow arriving at 13:34, which is closer to the his-

694 torical value of 13:30 than the 0.06 n base mode which arrived at 14:05 (difference of 35
 695 minutes). Further downstream, the Rexburg profile line logs the 0.03 n flow arriving at
 696 14:41, close to the historical value of 14:30. However, the base model (0.06 n) arrives at
 697 16:25, nearly 2 hours later – a significant difference. We recommend that future work
 698 involves a depth-variable Manning's roughness coefficient or a variable Manning's rough-
 699 ness coefficient throughout the domain, given that the Manning's sensitivity analysis showed
 700 that the roughness wholly affects the simulation and computational results.

701 Although previous studies demonstrated that the mesh could control a dam fail-
 702 ure flood solution, we conclude from the mesh sensitivity analysis that the mesh does
 703 not control or impact the solution of the Teton Dam flood wave arrival time or flow. With
 704 the low relief of the terrain (with Menan Butte and the Teton canyon as the only excep-
 705 tions), and the fairly high resolution cell-gridding, the mesh does not change the com-
 706 putational result. However, the geometry is a crucial source of potential error in any hy-
 707 draulic model with uncertainty. For example, having a higher resolution topography 5 m)
 708 rather than 10 m for the dam's reservoir could improve reservoir volume predictions to
 709 be closer to historical values.

710 Additionally, there is an uncertainty associated with the historical depth value, as
 711 they were not directly associated with a location (longitude and latitude) when collected
 712 in 1976. Therefore, with that data limitation, there is uncertainty associated with the
 713 historical values Table 2. Future work could include a survey in Eastern Idaho of remain-
 714 ing structures to document known high watermarks to improve this data limitation. Then,
 715 this uncertainty could be eliminated by integrating those locations as stationary gauges.

716 The HEC-RAS hydrologic model a widely used dam failure modeling software in
 717 the US. HEC-RAS in the past has been used to model the Teton Dam failure using the
 718 1D unsteady flow routing (1D SWE equations) to route an inflowing flood hydrograph
 719 through a reservoir (Land, 1980). In this project, we expand on previous research, em-
 720 ploying HEC-RAS v.5.0.7 2D unsteady flow routing capabilities (Full Momentum SWE)
 721 for comparison to GeoClaw. This study found both HEC-RAS and GeoClaw to produce
 722 similar numerical solutions and resultant simulations with numerical gauges depicting
 723 maximum flow depths and flood wave arrival times that largely agreed with historical
 724 data. With this study and the results, we would recommend using GeoClaw for forecast-
 725 ing or hindcasting downstream flow behavior from dam breach simulations.

726 5.1 Recommendations for Future Work

727 5.1.1 *Drone Photogrammetry Generated Topographies in Dam Failure* 728 *Modeling*

729 As some dams are in remote locations where only coarse DEMs exist, drone pho-
 730 togrammetry could be a valuable tool for creating supplemental high-resolution DEMs.
 731 We recommend that future work investigate high-resolution topography usage in Geo-
 732 Claw dam breach modeling, focusing on resolution and efficiency. Initial testing demon-
 733 strated that drone photogrammetry-generated topography could be uploaded into the
 734 HEC-RAS's RAS Mapper as a terrain in GeoTiff format. Through uploading the three
 735 raster data sets in this study, HEC-RAS can further import them within a single layer,
 736 which can be merged into a single raster. Using HEC-RAS or any ESRI product (Ar-
 737 cMap or ArcGIS Pro), exported combined terrains could be loaded into GeoClaw for a
 738 resolution and run-time efficiency-focused study.

739 5.1.2 *Teton Dam GeoClaw Model Manning's Coefficient*

740 This study recommends additional Manning's sensitivity analyses to be performed,
 741 comparing uniform Manning's n values which spatially varying Manning's roughness sen-
 742 sitivity analyses and depth-averaged Manning's n. Additionally, to improve uncertain-

ties in this model, we recommend quantifying the geomorphological differences in the canyon from 1976 pre-failure to the present day data as the volume of landslide debris that might be offsetting reservoir fill volume values in this study. Future work could involve simulation of a higher-resolution Teton Canyon (generated from drone photogrammetry as well) which might increase computation times, but could improve downstream canyon values.

5.1.3 Depth-Averaged Debris Modeling of Teton Dam failure

The current GeoClaw model uses the SWEs and Lagrangian particles to track streamlines. The massless Lagrangian particles could be further parameterized with mass, size, drag (function of particle Reynolds number), and buoyancy – the most significant forces acting on fluid objects. Through further parameterization, the user could model debris carried in the dam failure flood wave such as cattle, houses, sediment (sand), and timber. GeoClaw could use model development like COULWAVE and ComMIT/MOST(NOAA) to simulate buoyant debris. However, research explores the simulation of debris sourced from vegetation, vehicles, or non-buoyant debris (the additional parameterized Lagrangian gauges) such as buildings, sand, and rock. The Teton Dam failure provides an opportunity for future work in this area, which could help forecast dam failure risk and can assess costs as debris removal, improving community resilience.

Open Research

The study used open-source software HEC-RAS (USACE, 2019) and GeoClaw (Clawpack Development Team, 2021b) for 2D numerical modeling. The Teton Dam models (version used in this paper) are located on GitHub with a (i) README.md file that includes the metadata and a complete model description, (ii) configuration parameters along with the specific script and workflow which is preserved in the repository, and the (iii) code which can produce the data that supports the summary results, tables and figures (Spero, Hannah and Calhoun, Donna and Schubert, Michael, 2021). Additionally, this study used the high-performance computing support of the R2 compute cluster (DOI: 10.18122/B2S41H) provided by Boise State University's Research Computing Department (Boise State Research Computing, 2017).

Data Availability Statement

Both the (i) ASCII topography data used for creating the underlying terrain, and (ii) the GeoClaw and HEC-RAS project files are available at [GitHub: Spero-Hannah/Teton-Dam-Failure-Example] via [DOI: 10.5281/zenodo.586668, persistent identifier link] with [Berkeley Software Distribution (BSD) license]; (Spero, Hannah and Calhoun, Donna and Schubert, Michael, 2021). Unmodified topography files can be found on the USGS website (USGS, 2015).

CRediT Author Statement

The authors confirm contribution to the paper as follows: Conceptualization: D. Calhoun; Methodology: D. Calhoun, H. Spero; Software: D. Calhoun, H. Spero; Formal Analysis and Investigation: H. Spero; Resources: D. Calhoun, M. Schubert; Data Curation: D. Calhoun; Writing-Original Draft: H. Spero; Writing-Review and Editing: D. Calhoun, M. Schubert; Funding Acquisition: D. Calhoun, H. Spero. All authors reviewed the results and approved the final version of the manuscript.

786 **Acknowledgments**

787 The Authors would like to thank Boise State University's Boise Center Aerospace Lab-
 788 oratory (BCAL) for access to software, the Idaho Technical Committee of the Northwest
 789 Regional Floodplain Managers Association (ITC-NORFMA), and others for their involve-
 790 ment and support of this research. The Authors would like to thank the Bureau of Recla-
 791 mation and the Department of the Interior for allowing access and reproduction of their
 792 drone photogrammetry data and historical records. Further, the Authors would like to
 793 thank both Dr. Jim McNamara (thesis committee member) and the staff at HDR En-
 794 gineering Inc. for their respective internal reviews of the manuscript. *Land Acknowledge-*
 795 *ment* The Authors also acknowledge that the Teton River Canyon site area was home
 796 to the Shoshone and Bannock Indian people in the early 1800s. Per the "The Policy of
 797 the Shoshone-Bannock Tribes for Management of Snake River Basin Resources" the Shoshone-
 798 Bannock Tribes are acknowledged as the previous owners of the ceded lands of the Teton
 799 River Canyon study area (Reclamation, 2006).

800 **Funding Acknowledgements:** This work was supported by D. Calhoun's Na-
 801 tional Science Foundation [#1819257, 2018], "Parallel, adaptive Cartesian grid algorithms
 802 for natural hazards modeling"; H. Spero's Association of State Floodplain Managers stu-
 803 dent scholarship [2020]. Broader impacts of this research, a Virtual Reality Teton Dam
 804 environment, was awarded to H. Spero from Boise State University's Undergraduate Re-
 805 search and Creative Activities Grant 2021 (URCA).

806 **References**

- 807 Ackerman, C., Fleming, M., & Brunner, G. (2008). Hydrologic and Hydraulic Mod-
 808 els for Performing Dam Break Studies. In *World Environmental and Water Re-*
 809 *sources Congress 2008: Ahupua'A* (pp. 1–11).
- 810 Almassri, B. (2011). *Numerical Simulation Analysis of Dam Breaks using ISIS &*
 811 *HEC-RAS* (Unpublished doctoral dissertation). Palenstine Polytechnic Univer-
 812 sity.
- 813 Arcos, M., & LeVeque, R. J. (2015). Validating Velocities in the GeoClaw Tsunami
 814 Model Using Observations Near Hawaii from the 2011 Tohoku Tsunami. *Pure*
 815 *and Applied Geophysics*, 172(3), 849–867.
- 816 ASCE. (2021). Edenville and Sanford Dam Failures: Field Reconnaissance Report..
- 817 ASDSO. (2021). *Dam Failures and Incidents*.
- 818 Aureli, F., Maranzoni, A., & Petaccia, G. (2021). Review of Historical Dam-Break
 819 Events and Laboratory Tests on Real Topography for the Validation of Numer-
 820 ical Models. *Water*, 13(14), 1968.
- 821 Balloffet, A., & Scheffler, M. (1982). Numerical Analysis of the Teton Dam Failure
 822 Flood. *Journal of Hydraulic Research*.
- 823 Begnudelli, L., & Sanders, B. (2007). Simulation of the St. Francis Dam-Break
 824 Flood. *Journal of Engineering Mechanics*, 133(11), 1200–1212.
- 825 Berger, M., George, D., LeVeque, R., & Mandli, K. (2011). The GeoClaw Software
 826 for Depth-Averaged Flows with Adaptive Refinement. *Advances in Water Re-*
 827 *sources*, 34(9), 1195–1206.
- 828 Bhandari, M. (2017). *One-Dimensional (1D) & Two-Dimensional (2D) Dam Break*
 829 *Analysis and Comparison of Different Breaching Parameters using HEC-RAS*.
 830 Southern Illinois University at Carbondale.
- 831 Biscarini, C., Di Francesco, S., Ridolfi, E., & Manciola, P. (2016). On the Simulation
 832 of Floods in a Narrow Bending Valley: The Malpasset Dam Break Case Study.
 833 *Water*, 8(11), 545.
- 834 Blanton, J. (1977). Floodplain Inundation Caused by Dam Failure. In *Proceedings of*
 835 *Dam-Break Flood Routing Model Workshop*.
- 836 Boise State Research Computing. (2017). *R2: Dell HPC Intel E5v4 (High Perfor-*
 837 *mance Computing Cluster)*. Boise State University Boise (ID).

- Bosa, S., & Petti, M. (2011). Shallow Water Numerical Model of the Wave Generated by the Vajont Landslide. *Environmental Modelling & Software*, 26(4), 406–418.
- Boulange, J., Hanasaki, N., Yamazaki, D., & Pokhrel, Y. (2021). Role of Dams in Reducing Global Flood Exposure Under Climate Change. *Nature Communications*, 12(1), 1–7.
- Brown, R. (1977). A Simulation of the Hydraulic Events During and Following the Teton Dam Failure. In *Proceedings of Dam-Break Flood Routing Model Workshop*.
- Brunner, G. (2002). HEC-RAS (River Analysis System). In *North American Water and Environment Congress & Destructive Water* (p. 3782-3787).
- Brunner, G. (2016). Benchmarking of the HEC-RAS Two-Dimensional Hydraulic Modeling Capabilities. *US Army Corps of Engineers—Hydrologic Engineering Center*, 1-116.
- Calhoun, D., & Burstedde, C. (2017). ForestClaw: A Parallel Algorithm for Patch-Based Adaptive Mesh Refinement on a Forest of Quadtrees. *arXiv preprint arXiv:1703.03116*.
- Capasso, S., Tagliafierro, B., Güzel, H., Yilmaz, A., Dal, K., Kocaman, S., ... Evangelista, S. (2021). A Numerical Validation of 3D Experimental Dam-Break Wave Interaction with a Sharp Obstacle Using DualSPHysics. *Water*, 13(15), 2133.
- Carter, B. (1976). Field Inspection of Shallow Slides on the Teton Reservoir. *Teton Project, Idaho, Reclamation Memorandum from Regional Director, Boise, Idaho, to Director of Design and Construction Engineering and Research Center, Denver, Colorado*.
- Chow, T. (1959). *Open Channel Hydraulics*. McGraw-Hill Civil Engineering Series McGraw-Hill: Toronto.
- CivilGEO. (2021). *HEC-RAS 2D Flow Modeling*. Retrieved from <https://knowledge.civilgeo.com/knowledge-base/hec-ras-2d-flow-area-modeling/>
- Clawpack Development Team. (2020). *Clawpack (GeoClaw) Software*. Retrieved from <http://www.clawpack.org> (Version 5.7.1) doi: <https://doi.org/10.5281/zenodo.4025432>.
- Clawpack Development Team. (2021a). *Clawpack-5 Lagrangian Gauges for Particle Tracking*. Retrieved from http://www.clawpack.org/lagrangian_gauges.html
- Clawpack Development Team. (2021b). *Clawpack v5.8.0 Release Notes*. Retrieved from <http://doi.org/10.5281/zenodo.4503024>
- Costabile, P., Costanzo, C., Ferraro, D., Macchione, F., & Petaccia, G. (2020). Performances of the New HEC-RAS Version 5 for 2D Hydrodynamic-Based Rainfall-Runoff Simulations at Basin Scale: Comparison with a State-of-the art Model. *Water*, 12(9), 2326.
- Dasallas, L., Kim, Y., & An, H. (2019). Case Study of HEC-RAS 1D-2D Coupling Simulation: 2002 Baeksan Flood Event in Korea. *Water*, 11(10), 2048.
- Fread, D. (1977). The Development and Testing of a Dam-Break Flood Forecasting Model. In *Proceedings of Dam-Break Flood Routing Model Workshop*.
- Gallegos, H., Schubert, J., & Sanders, B. (2009). Two-Dimensional, High-Resolution Modeling of Urban Dam-Break Flooding: A Case Study of Baldwin Hills, California. *Advances in Water Resources*, 32(8), 1323-1335. Retrieved from <https://www.sciencedirect.com/science/article/pii/S0309170809000815> doi: <https://doi.org/10.1016/j.advwatres.2009.05.008>
- Garcia-Martinez, N., Gonzalez-Ramirez, & O'Brien, J. (2009). Dam-Break Flood Routing. *WIT Transactions on State-of-the-art in Science and Engineering*, 36.
- George, A., & Nair, B. T. (2015). Dam Break Analysis Using BOSS DAMBRK.

- 893 *Aquatic Procedia*, 4, 853-860. Retrieved from <https://www.sciencedirect.com/science/article/pii/S2214241X1500108X>. (International Conference
 894 On Water Resources, Coastal and Ocean Engineering: ICWRCOE'15) doi:
 895 <https://doi.org/10.1016/j.aqpro.2015.02.107>
- 896 George, D. (2011). Adaptive Finite Volume Methods with Well-Balanced Riemann
 897 Solvers for Modeling Floods in Rugged Terrain: Application to the Malpas-
 898 set Dam-Break Flood (France, 1959). *International Journal for Numerical
 899 Methods in Fluids*, 66(8), 1000–1018.
- 900 González, F., LeVeque, R., Chamberlain, P., Hirai, B., Varkovitzky, J., & George,
 901 D. (2011). Validation of the GeoClaw Model. In *NTHMP MMS Tsunami
 902 Inundation Model Validation Workshop*. *GeoClaw Tsunami Modeling Group*.
- 903 Gundlach, D., & Thomas, W. (1977). *Guidelines for Calculating and Routing a
 904 Dam-Break Flood* (No. 5). Department of Defense, Department of the Army,
 905 Corps of Engineers.
- 906 Hervouet, J.-M., & Petitjean, A. (1999). Malpasset Dam-Break Revisited with Two-
 907 Dimensional Computations. *Journal of Hydraulic Research*, 37(6), 777-788.
- 908 Hu, H., Zhang, J., & Li, T. (2018). Dam-break flows: Comparison between flow-3d,
 909 mike 3 fm, and analytical solutions with experimental data. *Applied Sciences*,
 910 8(12). Retrieved from <https://www.mdpi.com/2076-3417/8/12/2456> doi: 10
 911 .3390/app8122456
- 912 Keefer, T., & Simons, R. (1977). Qualitative Comparison of Three Dam Break
 913 Routing Models. In *Proceedings of Dam-Break Flood Routing Model Work-
 914 shop*.
- 915 Kocaman, S., Evangelista, S., Guzel, H., Dal, K., Yilmaz, A., & Viccione, G. (2021).
 916 Experimental and Numerical Investigation of 3D Dam-Break Wave Propaga-
 917 tion in an Enclosed Domain with Dry and Wet Bottom. *Applied Sciences*,
 918 11(12), 5638.
- 919 Kumar, S., Jaswal, A., Pandey, A., & Sharma, N. (2017). Literature Review of Dam
 920 Break Studies and Inundation Mapping using Hydraulic Models and GIS. *In-
 921 ternational Research Journal of Engineering and Technology*, 4(5), 55–61.
- 922 Land, L. (1980). *Evaluation of Selected Dam-Break Flood-Wave Models by Using
 923 Field Data*. US Geological Survey (USGS) Water-Resources Investigations 80-
 924 44. NSTL Station, MS 39529, US. Retrieved from https://digital.library.unt.edu/ark:/67531/metadc967916/m2/1/high_res_d/report.pdf
- 925 LeVeque, R. J. (2002). *Finite Volume Methods for Hyperbolic Problems*. Cambridge
 926 University Press.
- 927 Loza, A. R. A., & Fidélis, T. (2021). Literature Review on the Analysis of Climate
 928 Change Risks in the Environmental Impact Assessment of Dams. *Impact As-
 929 essment and Project Appraisal*, 1–13.
- 930 Macchione, F., & Sirangelo, B. (1990). Floods Resulting from Progressively
 931 Breached Dams. *Hydrology in Mountainous Regions. II-Artificial Reservoirs;
 932 Water and Slopes*, 325-332.
- 933 MacInnes, B., Gusman, A., LeVeque, R., & Tanioka, Y. (2013). Comparison of
 934 Earthquake Source Models for the 2011 Tohoku Event Using Tsunami Simu-
 935 lations and Near-Field Observations. *Bulletin of the Seismological Society of
 936 America*, 103(2B), 1256–1274.
- 937 Magley, D. (1981). Post Failure Landslides. *Teton Reservoir, Minidoka Project,
 938 Idaho, US Department of the Interior, Water and Power Resources Service,
 939 Boise, Idaho*.
- 940 Mandli, K., & Dawson, C. (2014). Adaptive Mesh Refinement for Storm Surge.
 941 *Ocean Modelling*, 75, 36-50.
- 942 Martin, C., & Zovne, J. (1971). Finite-Difference Simulation of Bore Propagation.
 943 *Journal of the Hydraulics Division*, 97(7), 993-1010.
- 944 Nagel, A., & Ptak, T. (2021). Approaching Obsolescence? A Multi-Criteria Analysis
 945 of High-Risk Dams in the United States Pacific Northwest. *International Jour-*
 946 *n*

- nal of Water Resources Development, 1-25.
- Néelz, S., Pender, G., et al. (2010). Benchmarking of 2D Hydraulic Modelling Packages.
- Patel, D. P., Ramirez, J. A., Srivastava, P. K., Bray, M., & Han, D. (2017). Assessment of Flood Inundation Mapping of Surat City by Coupled 1D/2D Hydrodynamic Modeling: A Case Application of the New HEC-RAS 5. *Natural Hazards*, 89(1), 93–130.
- Pierce, K., Morgan, L., Link, P., Kuntz, M., & Platt, L. (1992). The Track of the Yellowstone Hot Spot: Volcanism, Faulting, and Uplift. *Regional Geology of Eastern Idaho and Western Wyoming: Geological Society of America Memoir*, 179(322), 1-53.
- Price, J. (2004). Topics in Fluid Dynamics: Dimensional Analysis, the Coriolis force, and Lagrangian and Eulerian Representations. *MIT DSpace (Digital Repository)*. Retrieved from <http://hdl.handle.net/1721.1/79879>
- Psomiadis, E., Tomanis, L., Kavvadias, A., Soulis, K. X., Charizopoulos, N., & Michas, S. (2021). Potential Dam Breach Analysis and Flood Wave Risk Assessment using HEC-RAS and Remote Sensing Data: A Multicriteria Approach. *Water*, 13(3), 364.
- Reclamation. (1976). *Report to the US Department of the Interior and State of Idaho on Failure of Teton Dam*. US Department of the Interior, Bureau of Reclamation.
- Reclamation. (2000). *Geomorphology and River Hydraulics of the Teton River Upstream of Teton Dam, Teton River, Idaho*. US Department of the Interior, Bureau of Reclamation.
- Reclamation. (2006). *Teton River Resource Management Plan*.
- Reclamation. (2008). *The Teton Dam Failure - An Effective Warning and Evacuation*. Retrieved from https://damfailures.org/wp-content/uploads/2015/07/075_The-Teton-Dam-Failure.pdf
- Shigeeda, M., Akiyama, J., Ura, M., & Arita, Y. (2001). 2D Numerical Model Based on Unstructured Finite Volume Method for Flood Flows. *Proceedings of Hydraulic Engineering*, 45, 895-900.
- Shrestha, A., Bhattacharjee, L., Baral, S., Thakur, B., Joshi, N., Kalra, A., & Gupta, R. (2020). Understanding Suitability of MIKE 21 and HEC-RAS for 2D Floodplain Modeling. In *World Environmental and Water Resources Congress 2020: Hydraulics, Waterways, and Water Distribution Systems Analysis* (pp. 237–253).
- Smith, C., Prescott, S., Ryan, E., Calhoun, D., Sampath, R., Anderson, D., & Casteneda, C. (2015). *Flooding Capability for River-Based Scenarios* (Tech. Rep.). Idaho Falls, Idaho, US: Idaho National Lab.(INL).
- Snyder, F. (1977). Floods from Breaching of Dams. In *Proceedings of Dam-Break Flood Routing Model Workshop*.
- Solava, S., & Delatte, N. (2003). Lessons from the Failure of the Teton Dam. In *Forensic Engineering* (p. 178-189).
- Spero, H., & Calhoun, D. (2020). Modeling the Downstream Consequences of the 1976 Teton Dam Failure and Resulting Flood by Validating the GeoClaw Software with Historical Data. *Annual Association of State Floodplain Managers Collegiate Student Paper Competition*.
- Spero, Hannah and Calhoun, Donna and Schubert, Michael. (2021). *Teton Dam Repository v.1.0.1*. Retrieved from <https://zenodo.org/badge/latestdoi/435099256> doi: 10.5281/zenodo.5806668
- Stanford University. (2018). *National Performance of Dams Program*. Department of Civil & Environmental Engineering. Retrieved from <https://npdp.stanford.edu/sites/default/files/reports/npdp>
- Strelkoff, T., Schamber, D., & Katopodes, N. (1977). Comparative Analysis of Routing Techniques for the Floodwave from a Ruptured Dam. In *Proceedings*

- of Dam-Break Flood Routing Model Workshop.
- Thomas, W. (1977). Calculating and Routing the Teton Dam-Break Flood. In *United States Water Resources Council*.
- Turzewski, M., Huntington, K., & LeVeque, R. (2019). The Geomorphic Impact of Outburst Floods: Integrating Observations and Numerical Simulations of the 2000 Yigong Flood, Eastern Himalaya. *Journal of Geophysical Research: Earth Surface*, 124(5), 1056-1079.
- Urzică, A., Mihu-Pintilie, A., Stoleriu, C. C., Cîmpianu, C. I., Huțanu, E., Pricop, C. I., & Grozavu, A. (2021). Using 2D HEC-RAS Modeling and Embankment Dam Break Scenario for Assessing the Flood Control Capacity of a Multi-Reservoir System (NE Romania). *Water*, 13(1), 57.
- USACE. (2019). Retrieved from https://www.hec.usace.army.mil/software/hec-ras/documentation/HEC-RAS_5.0.7_Release_Notes.pdf
- USGS. (1976). *Teton Dam Flood of June 1976*. (Map 1:24,000 scale)
- USGS. (2015). *United States Geological Survey of the US Department of the Interior. Eastern Idaho Topography: US Geological Survey database at 10m and 30 m resolution*. Retrieved from dd.cr.usgs.gov
- USGS. (2021). *United States Geological Survey Gage 13056500 Henry's Fork Near Rexburg, Idaho*. Retrieved from https://nwis.waterdata.usgs.gov/id/nwis/peak/?site_no=13056500&agency_cd=USGS
- Valiani, A., Caleffi, V., & Zanni, A. (2002). Case Study: Malpasset Dam-Break Simulation Using a Two-Dimensional Finite Volume Method. *Journal of Hydraulic Engineering*, 128(5), 460-472.
- Williams, P. L., Covington, H., & Pierce, K. L. (1982). Cenozoic Stratigraphy and Tectonic Evolution of the Raft River Basin, Idaho. *Cenozoic Geology of Idaho: Idaho Bureau of Mines and Geology Bulletin*, 26, 491-504.
- Wurbs, R. A. (1987). Dam-Breach Flood Wave Models. *Journal of Hydraulic Engineering*, 113(1), 29-46.
- Yakti, B. P., Adityawan, M. B., Farid, M., Suryadi, Y., Nugroho, J., & Hadihardaja, I. K. (2018). 2D Modeling of Flood Propagation Due to the Failure of Way Ela Natural Dam. In *MATEC Web of Conferences* (Vol. 147).
- Yi, X. (2011). A Dam Break Analysis using HEC-RAS. *Journal of Water Resource and Protection*, 2011.
- Yochum, S., Goertz, L., & Jones, P. (2008). Case Study of the Big Bay Dam Failure: Accuracy and Comparison of Breach Predictions. *Journal of Hydraulic Engineering*, 134(9), 1285-1293.